# Lifetime-broadening-suppressed/free XANES spectroscopy by high-resolution resonant inelastic x-ray scattering

Hisashi Hayashi,* Rumi Takeda, and Yasuo Udagawa
*IMRAM, Tohoku University, Katahira, Sendai 980-8577, Japan*

Tetsuya Nakamura,† Hayato Miyagawa,† Hironobu Shoji,‡ and Susumu Nanao
*Institute of Industrial Science, University of Tokyo, Komaba 4-6-1, Meguro, Tokyo 153-8505, Japan*

Naomi Kawamura
*JASRI, Mikazuki, Hyogo 679-5198, Japan*

The resonant inelastic x-ray scattering (RIXS) spectrum is uniquely related to the x-ray absorption oscillator strength distribution by the Kramers-Heisenberg equation via lifetime widths of the states involved. In this work it is shown that x-ray absorption near-edge structure (XANES), where the lifetime broadening of $1s$ core holes is suppressed and that of the $2p$ hole determines the resolution, can be analytically deduced from RIXS spectra. Furthermore, it is demonstrated that numerical procedures can provide lifetime-broadening-*free* (LBF) XANES, where the remaining $2p$ broadening is also eliminated. As examples, lifetime-broadening-suppressed (LBS) XANES and LBF-XANES of CuO and $CuCl_2 \cdot 2H_2O$ are derived from RIXS spectra measured by the use of a third-generation synchrotron source SPring-8 and are compared with XANES obtained by other methods to discuss the significance of LBS and LBF XANES spectroscopy.

## I. INTRODUCTION

X-ray absorption near-edge structure (XANES) provides one of the most useful tools for studying the density of unoccupied electron states and the symmetry of local structures around selected atomic species. XANES features are, however, often smeared out because of the natural width that originates from the finite lifetimes of core holes. The energy width increases as the atomic number ($Z$) increases, and for the $K$ shell it ranges from 1 eV ($V$, $Z=22$) up to 40 eV ($W$, $Z=74$).[1]

In order to overcome this limitation, high-resolution fluorescent excitation (HRFE) spectroscopy has been proposed to obtain lifetime-broadening-suppressed (LBS) XANES spectra,[2] where highly monochromatic incident x-ray energy is scanned across an absorption edge while monitoring the characteristic fluorescent x rays with better resolution than the natural lifetime width. However, later it was suggested that, rigorously speaking, HRFE spectra cannot be viewed as genuine LBS-XANES.[3–5] In addition, this technique is limited to atomic species where suitable high-resolution crystal analyzers are available for the characteristic lines.[2,4]

An alternative method of obtaining LBS-XANES by the use of resonant inelastic x-ray scattering (RIXS) has been theoretically suggested by Tulkki and Åberg[6] even before the proposition of the HRFE spectroscopy. They have stated that "the shape of the spectrum of the scattered photons may be used to disentangle bound-state excitations from continuous absorption more effectively than in ordinary absorption spectroscopy." However, although two attempts using conventional Cu $K\alpha$ x-ray sources can be found in literatures,[7,8] to the best of our knowledge, substantiation of their prediction by the use of modern synchrotron radiation has never been provided.

In previous reports we have studied RIXS spectral changes with excitation energies on several copper compounds.[9–12] It was observed that RIXS spectra approach the mirror image of XANES as the excitation energy decreases from the absorption edge and that the RIXS spectrum at the excitation energy $\geq 10$ eV below the edge is almost equivalent to $1s$ core-hole lifetime-broadening-suppressed XANES.[12] However, the $\geq 10$ eV off-resonant condition reduces the scattering intensity by almost 3 orders of magnitude than that attainable at resonant conditions. Hence it is much more preferable if LBS-XANES can be deduced from RIXS spectra obtained under close-to-resonant conditions.

In this work detailed RIXS spectra of CuO and $CuCl_2 \cdot 2H_2O$ are presented, procedures to extract $1s$ lifetime-broadening-suppressed and $1s$ as well as $2p$ lifetime-broadening-suppressed or lifetime-broadening-free (LBF) XANES from RIXS spectra are described, spectra thus obtained are compared with those by conventional absorption and HRFE spectroscopy, and advantages of the present methods are discussed.

## II. THEORETICAL

The differential cross section of the $1s2p$ RIXS process illustrated in Fig. 1(a) can be deduced from the well-known Kramers-Heisenberg equation as follows:[6]

$$\frac{d\sigma(\omega_1)}{d\omega_2} = 2\pi r_0^2 \int \frac{(\omega_2/\omega_1)(\Omega_{1s}-\Omega_{2p})(\Omega_{1s}+\omega)g_{2p,1s}(dg_{1s}/d\omega)(\Gamma_{2p}/2\pi\hbar)}{[(\Omega_{1s}+\omega-\omega_1)^2+\Gamma_{1s}^2/4\hbar^2][(\Omega_{2p}+\omega_2+\omega-\omega_1)^2+\Gamma_{2p}^2/4\hbar^2]} d\omega. \tag{1}$$
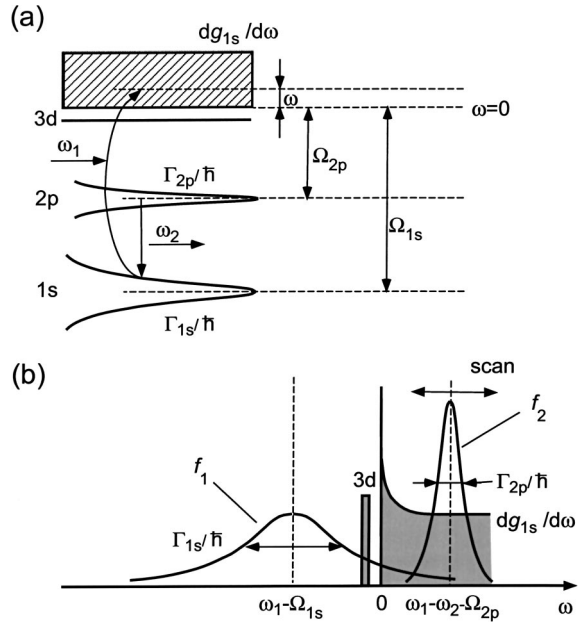
FIG. 1. (a) A diagram of the $1s2p$ resonant inelastic x-ray scattering (RIXS) process and (b) schematic presentation of lifetime-broadening-suppressed measurements by $1s2p$ RIXS. See text.



FIG. 2. A schematic diagram of the experimental setup.

Here $\hbar\omega_1$ and $\hbar\omega_2$ are incident and scattered photon energies, $\hbar\omega$ refers to the kinetic energies of the excited electron or binding energy of the bound electron in the intermediate state, and $\Gamma_{1s}$ and $\Gamma_{2p}$ are the widths of the $1s$ and $2p$ levels, the energies of which are represented by $\hbar\Omega_{1s}$ and $\hbar\Omega_{2p}$. The oscillator strength of the $1s2p$ radiative transition is given by $g_{2p,1s}$, and $dg_{1s}/d\omega$ is the oscillator strength distribution for $K$ absorption, which is in general a superposition of discrete and continuous features.

The integrand of Eq. (1) is essentially the product of three functions having $\omega$ as a common variable: two Lorentzians $f_1$ centered at $\omega = \omega_1 - \Omega_{1s}$ with full width at half maximum (FWHM) $\Gamma_{1s}/\hbar$ and $f_2$ centered at $\omega = \omega_1 - \omega_2 - \Omega_{2p}$ with FWHM $\Gamma_{2p}/\hbar$ and $dg_{1s}/d\omega$. Let us assume that $\Gamma_{1s}$ is much larger than $\Gamma_{2p}$ and that $dg_{1s}/d\omega$ is characterized by a narrow discrete band corresponding to vacant $3d$ and a sharp white line near the absorption threshold followed by a continuum, which are reasonable approximations for the copper compounds studied here. The three functions along the $\omega$ axis can then be depicted schematically in Fig. 1(b) for arbitrarily chosen $\omega_1$ and $\omega_2$. The scattering intensity is determined by the overlap of these three functions.

In RIXS measurements, $\omega_1$ is fixed and the scattering intensity is monitored as a function of $\omega_2$, which is equivalent to sliding very sharp $f_2$ along the $\omega$ axis while keeping $f_1$ and $dg_{1s}/d\omega$ fixed in Fig. 1(b). Since the scattering intensity is governed by the overlap of these three functions, it will be obvious that the bandwidth of the RIXS spectra is dominated only by $\Gamma_{2p}$ and not by $\Gamma_{1s}$, because in the overlapping region $f_1$ forms just a gradually decreasing background. Hence the RIXS spectrum is essentially $dg_{1s}/d\omega$ convoluted with $f_2$ and accordingly the latter can be calculated from the former, as long as the small distortion by $f_1$ can be adequately taken into account. Further, if the influ-
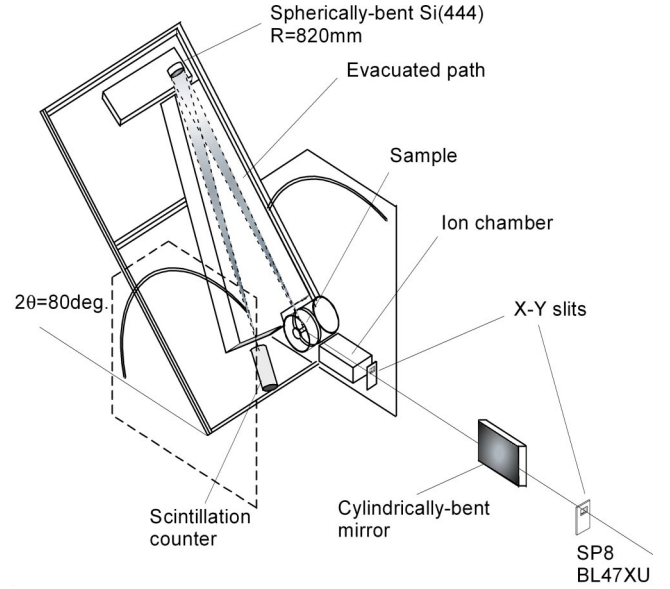
ence of $f_2$ can appropriately be estimated, it even is possible to deduce a $dg_{1s}/d\omega$ that is free from lifetime broadening due to both $\Gamma_{2p}$ and $\Gamma_{1s}$.

Incidentally, experimental conditions employed in the previous LBS studies can be understood by Fig. 1(b) in the following manner. In the case of the $\geqslant 10$ eV off-resonant condition,[12] $\omega_1 - \Omega_{1s}$ is much larger than $\Gamma_{1s}/2\hbar$, and accordingly $f_1$ levels off at $\omega > 0$ and can be considered to be a small constant. Under such a condition the RIXS spectrum itself is a convolution of $dg_{1s}/d\omega$ with $f_2$,[12] and hence LBS is achieved although the scattering intensity is low because of the small $f_1$ value. On the other hand, the HRFE spectroscopy[2,4] can be viewed as RIXS where $\omega_2$ is chosen to be $\Omega_{1s} - \Omega_{2p}$, making the center of $f_1$ and $f_2$ coincide to move both simultaneously. Thus the band width of HRFE spectra depends on both $\Gamma_{1s}$ and $\Gamma_{2p}$, although LBS is also achieved since the product of $f_1$ and $f_2$ is close to $f_2$.

## III. EXPERIMENT

The experiments were carried out at the BL47XU beamline at SPring-8. In this hard x-ray undulator beamline employed is a two-crystal dispersive Si(111) monochromator cooled with liquid nitrogen. The flux is believed to be about $10^{14}$ photons/sec, and the spectral width measured was about 0.9 eV at 8 keV.

The experimental setup is schematically shown in Fig. 2. The incident x rays were horizontally focused by a cylindrically bent mirror and irradiated onto the sample through a slit of 0.6 mm (width) $\times 0.2$ mm (height) and an ion chamber for monitoring the beam intensity. The scattered radiation was analyzed with a spherically bent 75-mm-diam Si(444) crystal having an 820 mm radius of curvature and detected by a scintillation counter. The beam path has 50-$\mu$m-thick Kapton windows and was evacuated by a scroll pump.

To acquire $1s2p$ RIXS spectra, the incident energy remained fixed and the scattered photon energy was analyzed

by moving the analyzer and detector synchronously. In these measurements, the active area of the analyzer was limited to 40 mm in diameter, which resulted in the overall energy resolution ($\Delta E_{exp}$) of 1.1 eV as determined by the FWHM of the elastic line. The total resolution is almost the same as that employed in our previous studies which was carried out at NSLS-X21,[11,12] although the bandwidth in incident x rays is different (0.2 eV, NSLS-X21; 0.9 eV, BL47XU). All data were taken on powder samples at room temperature at a constant scattering angle ($2\theta$) of 80°. The $2\theta$ direction was adopted because in this configuration $\Delta E_{exp}$ is little affected by the penetration depth of incident x rays.

Owing to the intense beam available at this beamline, the count rate in the present RIXS spectra is 3–4000 times higher than that in previous ones,[11,12] which makes detailed analysis of RIXS spectra possible.

The HRFE spectra were derived from the intensity at Cu $K\alpha_1$ energy, 8047.8 eV, of each RIXS spectrum. Conventional XANES spectra were obtained by monitoring the intensity of the total fluorescence by a $p$-$i$-$n$ photodiode while excitation energy is scanned.

## IV. RESULTS

Figures 3 and 4 show excitation energy dependence of the RIXS spectra of CuO and $CuCl_2 \cdot 2H_2O$ where the intensity is normalized by the peak height of the most intense band in each spectrum. The spectral shape changes with excitation energy significantly. The intensity also changes drastically with excitation energy. Hence the excitation energy dependences of the RIXS spectra are presented in Figs. 5 and 6 as two-dimensional contour maps where the two axes are the excitation energy and emitted photon energy, respectively. In Figs. 5 and 6 the normalization is made by the integrated intensity of the exciting x rays. Vertical cross sections of these two-dimensional plots correspond to the RIXS spectra in Figs. 3 and 4.

Excitation with x-ray energies well above the $K$-absorption-edge energy ($\sim 8986$ eV for CuO and $\sim 8988$ eV for $CuCl_2 \cdot 2H_2O$) yield a single band at 8047.8 eV, which is the well-known Cu $K\alpha_1$ fluorescence line. The band corresponding to $K\alpha_2$ fluorescence is out of the energy range of Figs. 3–6. As the excitation energy lowered, the two Cu compounds show substantially different spectral features.

In CuO, as the excitation energy lowered below the $K$-absorption edge, the main feature corresponding to the $K\alpha_1$ (denoted $A$) is shifted down with its width broadened. By lowering the excitation energy to $\sim 8983$ eV, a new branch, labeled $B$, becomes distinct. Another feature labeled $C$ is prominent at the excitation energy below 8983 eV. As the excitation energy further lowered, the peak energy of $A$ continues to shift to lower energy, preserving the energy loss ($E_{loss} = \hbar\omega_1 - \hbar\omega_2$) of 939 eV. At the same time, the scattering intensities decrease monotonously.

In contrast to the consecutive changes with excitation energy observed for $A$, branch $B$ is only observable within a small range of excitation energy, from $\sim 8981$ to $\sim 8984$ eV. Furthermore, the $E_{loss}$ of branch $B$ varies with the excitation energy as is evidenced from the difference in the slope of the
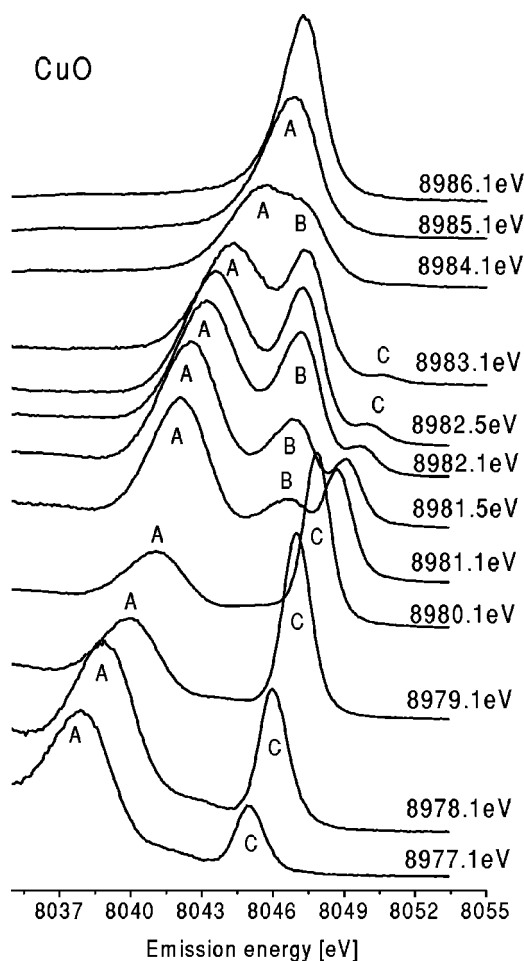


FIG. 3. Excitation energy dependence of resonant inelastic x-ray scattering (RIXS) spectra of CuO. The excitation energies are indicated in the figure.

two ridges in Fig. 5. On the other hand, $E_{loss}$ for $C$ remains constant (932 eV) and is independent of the excitation energy, as is branch $A$. As the excitation energy is tuned to $\sim 8980$ eV, which is the transition energy from $1s$ to the vacant $3d$,[13] band $C$ is the strongest with the bandwidth much narrower than the normal $K\alpha_1$ fluorescence.

In $CuCl_2 \cdot 2H_2O$, below the $K$-edge energy the main feature $A$ is shifted down with the decrease in excitation energy as is the case in CuO, but the branch corresponding to $B$ in CuO is barely observable. On the other hand, there is band $C$ at the high-energy side of $A$, and its behavior is similar to band $C$ of CuO. A part of these excitation energy dependences of RIXS spectral features have been already reported for CuO[11] and $CuCl_2 \cdot 2H_2O$.[12]

## V. DISCUSSION

What is observed by conventional XANES spectroscopy is the oscillator strength distribution convoluted with lifetime broadening due to $\Gamma_{1s}$, no matter how high the experimental resolution is. As was discussed in the previous section, the oscillator strength distribution $dg_{1s}/d\omega$, where the lifetime broadening due to $\Gamma_{1s}$ is suppressed and that due to $\Gamma_{2p}$
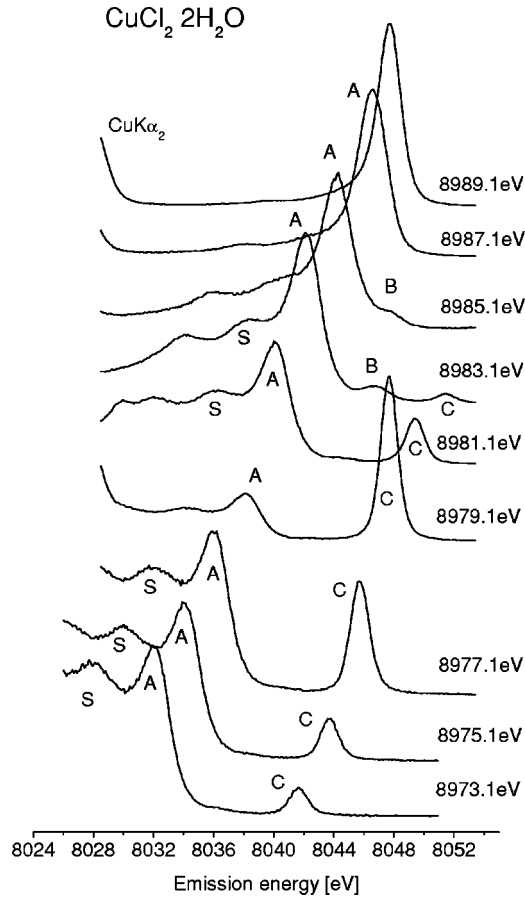
FIG. 4. Excitation energy dependence of resonant inelastic x-ray scattering (RIXS) spectra of $CuCl_2 \cdot 2H_2O$. The excitation energies are indicated in the figure.

determines the resolution, can in principle be deduced from RIXS. Moreover, it is also possible to remove the broadening due to $\Gamma_{2p}$ by numerical simulation. In the following the two procedures to derive LBS- and LBF-XANES are described.

### A. Analytical deduction of LBS-XANES from RIXS spectra

Under the approximation that $\Gamma_{2p}/2\hbar \ll 1$, Eq. (1) can be written using the $\delta$ function,
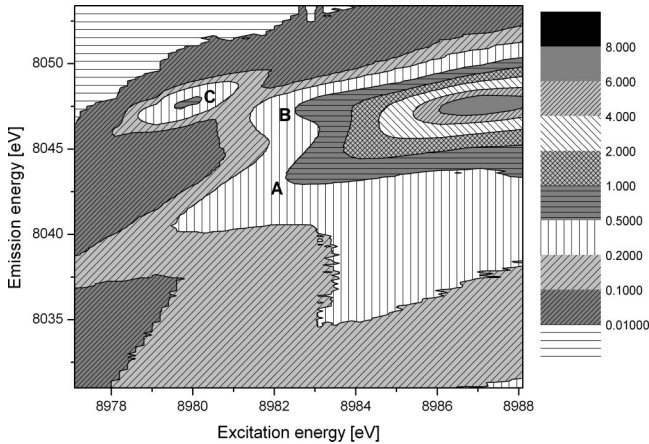


FIG. 5. Contour maps of the RIXS intensities of CuO as a function of the excitation energy and emission energy.



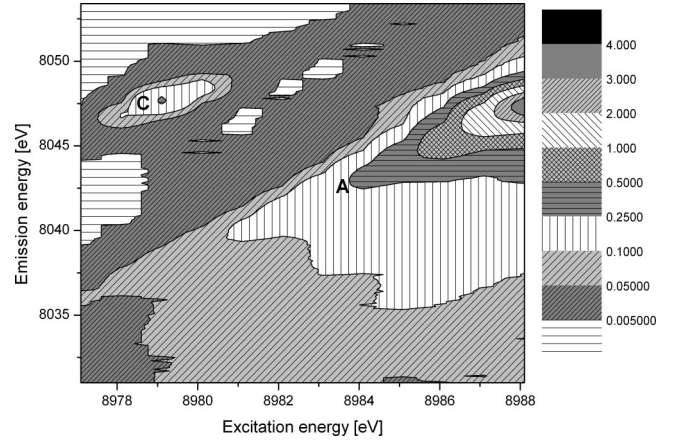FIG. 6. Contour maps of the RIXS intensities of $CuCl_2 \cdot 2H_2O$ as a function of the excitation energy and emission energy.

$$\frac{d\sigma(\omega_1)}{d\omega_2} \propto \int \frac{(\omega_2/\omega_1)(\Omega_{1s}-\Omega_{2p})(\Omega_{1s}+\omega)(dg_{1s}/d\omega)}{(\Omega_{1s}+\omega-\omega_1)^2+\Gamma_{1s}^2/4\hbar^2}$$
$$\times \delta(\Omega_{2p}+\omega_2+\omega-\omega_1)d\omega, \qquad (2)$$

which can be transformed to a more transparent form[7,8] by using the $K\alpha$-emission energy $\hbar\omega_{K\alpha1}=\hbar(\Omega_{1s}-\Omega_{2p})$ $=8047.8$ eV and the absorption energy $\omega_{abs}=\Omega_{1s}+\omega$ $=\omega_{K\alpha1}+\omega_1-\omega_2$:

$$\frac{d\sigma(\omega_1)}{d\omega_2} \propto \frac{(\omega_2/\omega_1)(\Omega_{1s}-\Omega_{2p})\omega_{abs}(dg_{1s}/d\omega_{abs})}{(\omega_{K\alpha1}-\omega_2)^2+\Gamma_{1s}^2/4\hbar^2}. \qquad (3)$$

This equation means that the cross section of $1s2p$ RIXS is, apart from the factor $(\omega_2/\omega_1)\omega_{abs}$, proportional to $dg_{1s}/d\omega_{abs}$ multiplied by a Lorentzian centered at $\omega_{K\alpha1}$. Hence it is possible to calculate $dg_{1s}/d\omega$ analytically from the experimental RIXS spectra directly or vice versa. Under the approximation employed here, $dg_{1s}/d\omega$ derived from RIXS by Eq. (3) is free from the lifetime broadening by $\Gamma_{1s}$ and the width is determined only by $\Delta E_{expt}$ and $\Gamma_{2p}$.

In the upper panel of Fig. 7, RIXS spectra of CuO excited at several excitation energies are shown. In the lower panel shown are LBS-XANES profiles of CuO analytically derived from the RIXS spectra by the use of Eq. (3). The inset shows the $1s \rightarrow 3d$ transition region below the absorption edge in an expanded scale. It is evident that, in spite of significant differences in the RIXS spectra employed, LBS-XANES derived by Eq. (3) almost overlaps with each other. Although not shown for clarity of the figure, use of RIXS spectra at other excitation energies produces almost the same results, as long as the excitation energy is below about 8984 eV.

LBS-XANES profiles calculated from some selected RIXS spectra of $CuCl_2 \cdot 2H_2O$ are shown in Fig. 8. Striking agreements among LBS-XANES deduced from very different RIXS spectra are again evident. In the case of $CuCl_2 \cdot 2H_2O$, RIXS spectra obtained at excitation energy lower than about 8985 eV produce almost the same LBS-XANES, reflecting the fact that the onset of the $K$ absorption is higher
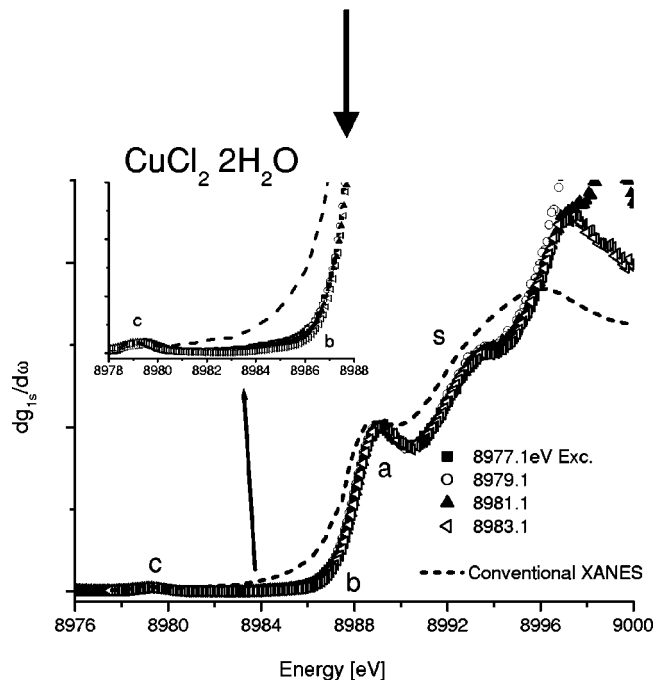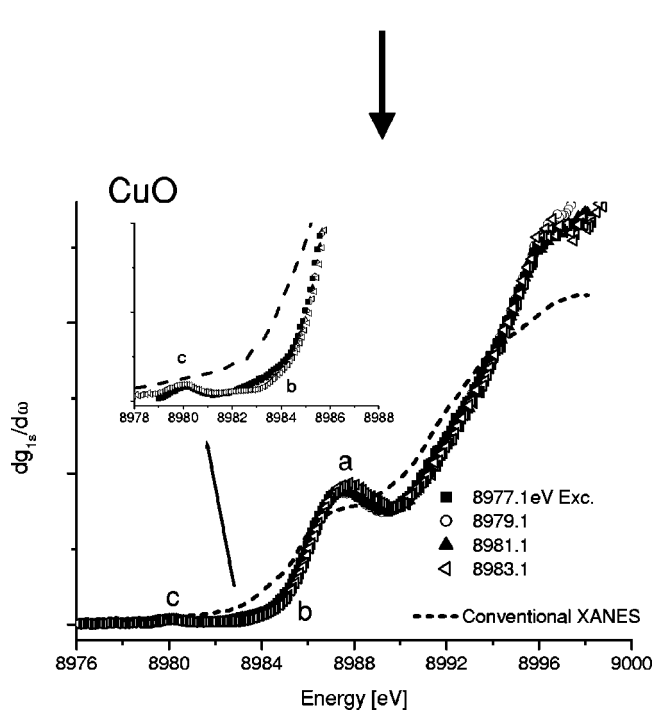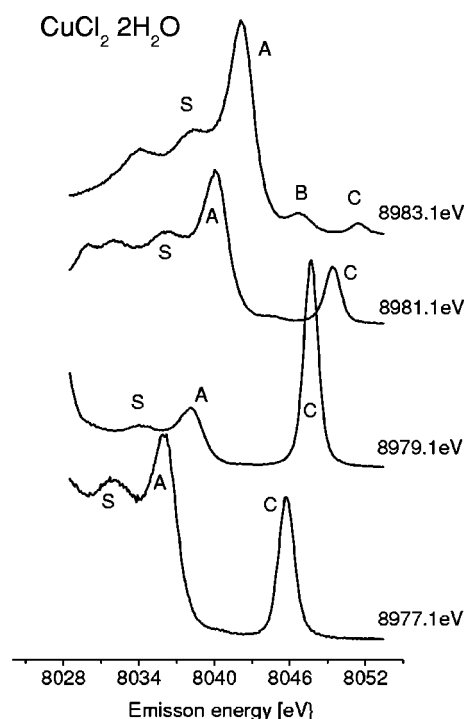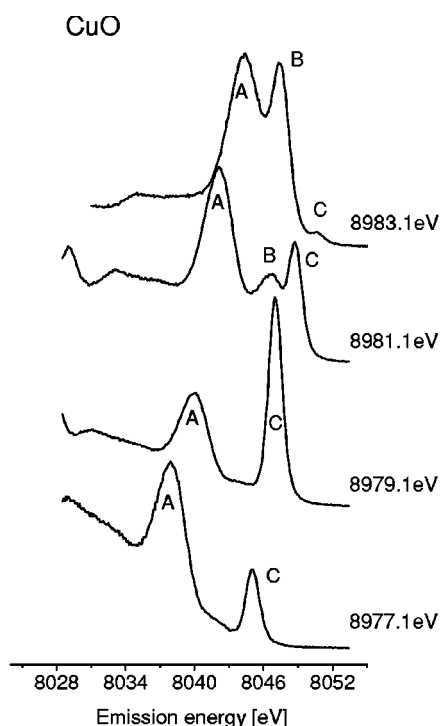
FIG. 7. Selected RIXS spectra (upper panel) and LBS-XANES profiles analytically calculated from them (lower panel) for CuO.



FIG. 8. Selected RIXS spectra (upper panel) and LBS-XANES profiles analytically calculated from them (lower panel) for $CuCl_2 \cdot 2H_2O$.

in energy than that of CuO.

In the lower panels of Figs. 7 and 8 conventional XANES are also shown. It is clear from the comparison that every feature in LBS-XANES is much more distinct than that in conventional XANES. For example, $1s \rightarrow 3d$ features, labeled by $c$, are clearly distinguished in LBS-XANES for both CuO and $CuCl_2 \cdot 2H_2O$, while they are not so distinct in the conventional XANES. The features labeled by

$a$, at 8987 eV in CuO and at 8989 eV in $CuCl_2 \cdot 2H_2O$, are recognized as a peak in the LBS-XANES, but they are just shoulders in the conventional XANES. These observations endorse that line broadening by $\Gamma_{1s}$, which often hampers detailed analysis of conventional XANES, is suppressed in LBS-XANES derived from RIXS. It is either $\Gamma_{2p}$ or $\Delta E_{expt}$ that determines the bandwidth of LBS-XANES derived from RIXS.

## B. Lifetime-broadening-free XANES by simulation

In the derivation of Eq. (3) it has been assumed that $\Gamma_{2p}$ is zero. Since the quality of the present RIXS data allows us to examine the profiles in detail numerically, attempted next is to derive $dg_{1s}/d\omega$ by numerical simulation based on Eq. (1) without such an assumption. The $dg_{1s}/d\omega$ profiles obtained from this procedure correspond to lifetime-broadening-*free* XANES.

To make analysis conditions closer to the experimental ones, self-absorption effects were taken into account by multiplying Eq. (1) by the well-known correction factor for infinitely thick samples, $1/(\mu_{inc}+\mu_{scat})$,

$$\frac{d\sigma(\omega_1)}{d\omega_2}=A\int\frac{(\omega_2/\omega_1)(\Omega_{1s}-\Omega_{2p})(\Omega_{1s}+\omega)(dg_{1s}/d\omega)}{[(\Omega_{1s}+\omega-\omega_1)^2+\Gamma_{1s}^2/4\hbar^2][(\Omega_{2p}+\omega_2+\omega-\omega_1)^2+\Gamma_{2p}^2/4\hbar^2)]}d\omega\frac{1}{\mu_{inc}+\mu_{scat}}. \tag{4}$$

In the calculation the absorption coefficient of incident x rays, $\mu_{inc}$, was estimated from the experimental data of Kosugi *et al.*,[13,14] and that of scattered x rays, $\mu_{scat}$, which is almost constant, was calculated from the atomic values.[15] The transition probability $g_{2p,1s}$ was assumed to be independent of both $\hbar\omega_1$ and $\hbar\omega_2$, and was included in the proportionality constant $A$. The values of $\Gamma_{1s}$ and $\Gamma_{2p}$ were set as 1.55 eV and 0.56 eV,[1] respectively. Various $dg_{1s}/d\omega$ models were assumed by modifying those obtained in the previous section; RIXS spectra were calculated by the use of Eq. (4) and compared with the observed ones, as will be discussed in detail in the next section. It may be fair to mention that the procedure described here does not result in a unique $dg_{1s}/d\omega$ profile. What endorses the results is only that every calculated RIXS spectrum by using a single $dg_{1s}/d\omega$ profile for various excitation energies reproduces the observed one well.

In Figs. 9(a) and 9(b), $dg_{1s}/d\omega$ models that reproduce observed RIXS spectra best are shown for CuO and $CuCl_2 \cdot 2H_2O$. Also shown are LBS-XANES profiles obtained in the previous section together with the HRFE spectra. It is evident that $dg_{1s}/d\omega$ obtained here shows much more distinct features than those obtained in the previous section and the HRFE spectra for both CuO and $CuCl_2 \cdot 2H_2O$, demonstrating that the core-hole lifetimes of $2p$ as well as $1s$ are removed. Well above the absorption edge the HRFE spectra show significant deviation from LBS-XANES, the reason for which we believe is in the reabsorption effects, as will be discussed later.

## C. RIXS spectra calculated from assumed oscillator strength distributions

In Fig. 10 calculated RIXS profiles from the $dg_{1s}/d\omega$ by analytical method ("LBS-XANES") are compared with experimental RIXS spectra at several excitation energies for CuO. Also shown are the calculated RIXS spectra by assuming conventional XANES spectra to represent $dg_{1s}/d\omega$ ("conventional XANES"). A similar comparison is made in Fig. 11 for $CuCl_2 \cdot 2H_2O$.

Above the threshold excitation the two $dg_{1s}/d\omega$ models generate similar bands at the energy of the regular $K\alpha_1$. As the excitation energy decreases from the threshold, conventional XANES spectra fail to reproduce the observed changes in RIXS features, giving $K\alpha$-like bands even with 8980.1 eV excitation. This is because conventional XANES spectra have a long tail to the low energy of the edge due to lifetime broadening by $\Gamma_{1s}$. On the other hand, RIXS spectra from
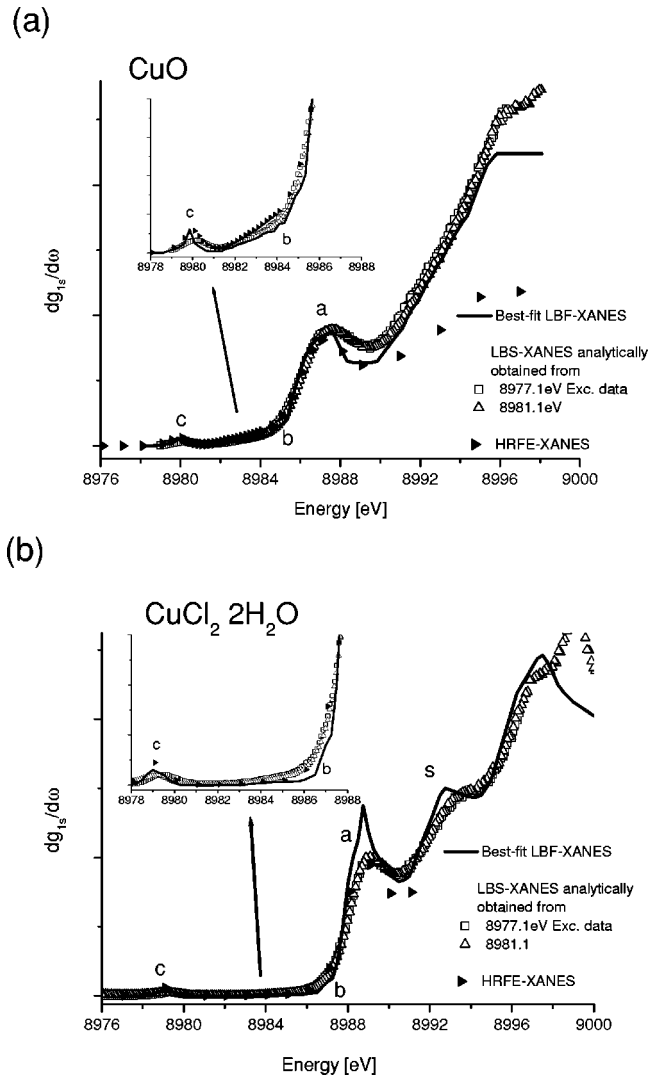
FIG. 9. The LBF-XANES ($dg_{1s}/d\omega$) obtained by the simulation method for (a) CuO and (b) $CuCl_2 \cdot 2H_2O$. Also shown are LBS-XANES spectra analytically obtained from RIXS by 8977.1 eV and 8981.1 eV excitation together with the HRFE spectra.
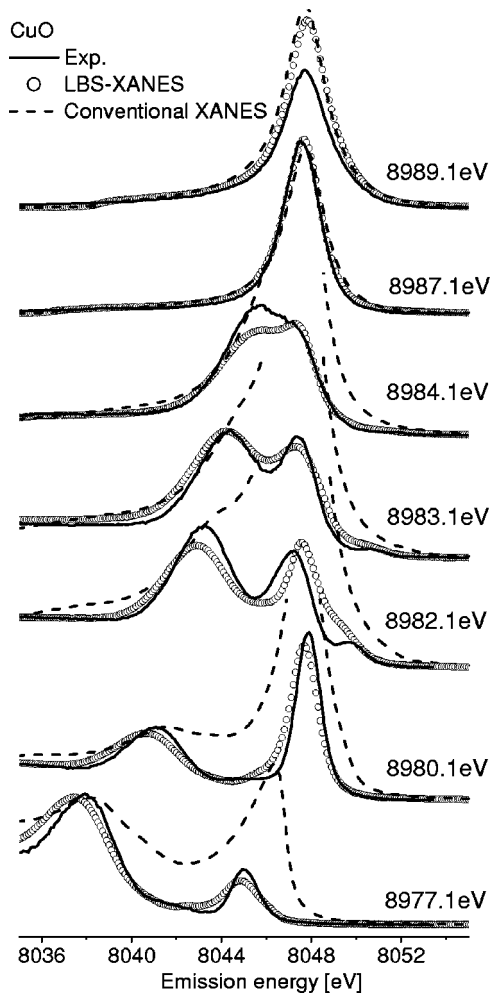
FIG. 10. Comparisons of the observed RIXS spectra and calculated ones by LBS-XANES analytically deduced from RIXS obtained with 8983.1 eV excitation ('LBS-XANES') for CuO. Also shown are RIXS calculated by the use of conventional XANES ("conventional XANES") as $dg_{1s}/d\omega$.
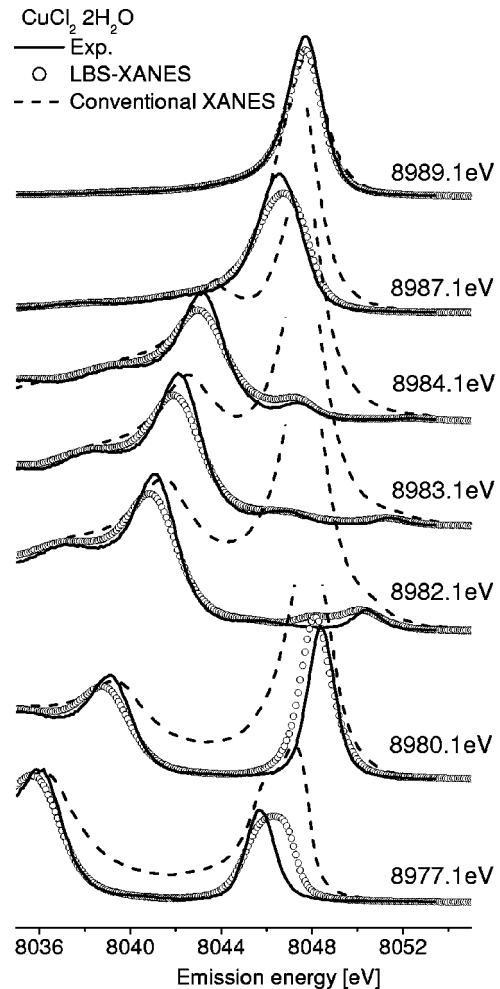


FIG. 11. Comparisons of the observed RIXS spectra and calculated ones by LBS-XANES analytically deduced from RIXS obtained with 8983.1 eV excitation ("LBS-XANES") for $CuCl_2 \cdot 2H_2O$. Also shown are RIXS calculated by the use of conventional XANES ("conventional XANES") as $dg_{1s}/d\omega$.

analytically derived $dg_{1s}/d\omega$, which is free from lifetime broadening by $\Gamma_{1s}$, almost overlap with observed ones as is evidenced from Figs. 10 and 11, demonstrating that RIXS spectra are heavily influenced by the lifetime-broadening width. A careful look at Figs. 10 and 11 reveals, however, that RIXS spectra by LBS-XANES show small but definite discrepancies from the observed ones. It is because lifetime broadening due to $\Gamma_{2p}$ is still involved in the analytically derived $dg_{1s}/d\omega$.

In Figs. 12 and 13 calculated RIXS profiles from the best-fit $dg_{1s}/d\omega$ models obtained from the simulations ["best-fit LBF-XANES" in Figs. 9(a) and 9(b)] are compared with experimental RIXS spectra. It is evident that the above-mentioned small discrepancies are nearly completely obliterated and the observed RIXS spectra, which vary enormously with excitation energy, almost exactly coincide with the corresponding ones generated by the *single $dg_{1s}/d\omega$* model for each compound. In fact, each $dg_{1s}/d\omega$ has been constructed in such a way that calculated RIXS spectra at various excitation energies reproduce all the observed ones. In the course

of the calculations it was noticed that the RIXS spectral shape is so sensitive to minute details of $dg_{1s}/d\omega$ that even a subtle change in the assumed $dg_{1s}/d\omega$ results in considerably different RIXS spectra at certain excitation energies.

Roughly speaking, there are the following relations between $dg_{1s}/d\omega$ features and RIXS peaks. First, the main RIXS features in CuO or $CuCl_2 \cdot 2H_2O$, which are indicated by $A$ in Figs. 3–8, are essentially determined by the profile of the prominent features in XANES indicated by $a$ in Figs. 7–9. The shape of the low-energy tail of the features $a$, indicated by $b$, determines the RIXS feature $B$; if the tail is rather steep as in the case of $CuCl_2 \cdot 2H_2O$, the RIXS feature $B$ is only barely observable. On the other hand, if the tail is long as conventional XANES, it makes an erroneous $K\alpha_1$-like band as are observed in the dashed lines in Figs. 10 and 11. The discrete $1s \rightarrow 3d$ band $c$ at 8980 eV for CuO and 8979 eV for $CuCl_2 \cdot 2H_2O$ is responsible to the prominent feature $C$ in the RIXS spectra. Under the exact resonance condition the bands $C$ have maximum intensity with peak energy of $\hbar\omega_{K\alpha1}$. In addition, a feature in $CuCl_2 \cdot 2H_2O$ de-
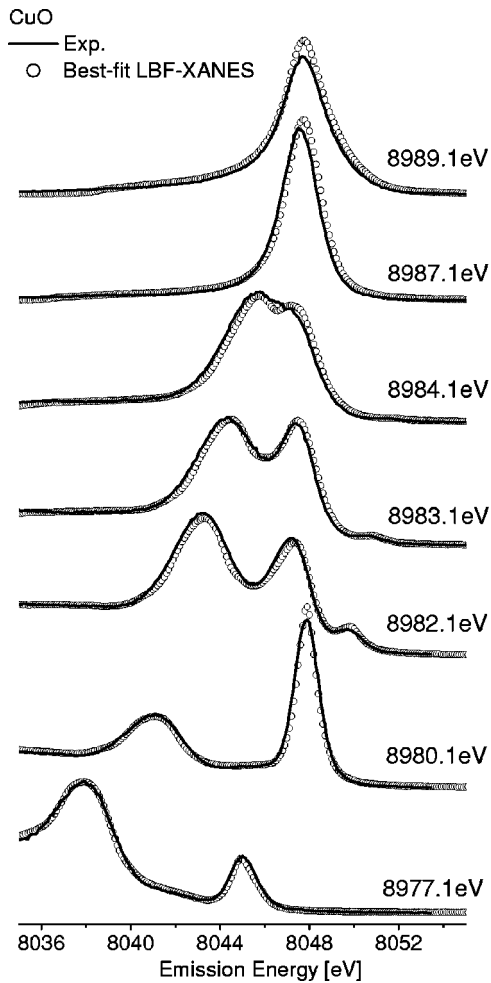
FIG. 12. Comparisons of the observed RIXS spectra and calculated ones by best-fit $dg_{1s}/d\omega$ models ("best-fit LBF-XANES") for CuO.



FIG. 13. Comparisons of the observed RIXS spectra and calculated ones by best-fit $dg_{1s}/d\omega$ models ("best-fit LBF-XANES") for $CuCl_2 \cdot 2H_2O$.

noted by $s$ in Figs. 8 and 9(b), which is missing in CuO, makes the feature $S$ in the RIXS of $CuCl_2 \cdot 2H_2O$. Band $S$ is not so prominent and only slightly noticeable on the continuum, since band $s$ is well above the threshold and hence the energy denominator in Eqs. (3) or (4) is rather large. This demonstrates that the RIXS method is particularly effective for studying XANES around the $K$ edge including the pre-edge region.

From the results presented here, the fundamental assumptions that the RIXS profiles are determined just by the three functions $f_1$, $f_2$, and $dg_{1s}/d\omega$ and the energy dependence of the $g_{2p,1s}$ is negligible are confirmed.[6] The complicated behavior of the RIXS spectra, found in Figs. 3–6, can be explained completely as the reflection of their LBF-XANES profiles. The "best-fit LBF-XANES" models shown in Fig. 9, which can reproduce RIXS almost completely as shown in Figs. 12 and 13, are indeed free from lifetime broadenings.

### D. LBS/LBF-XANES by RIXS and LBS-XANES by HRFE

In the previous study[12] we have shown that, if measured under $\geq 10$ eV off-resonant conditions, the RIXS spectrum itself is almost equivalent to LBS-XANES. However, the
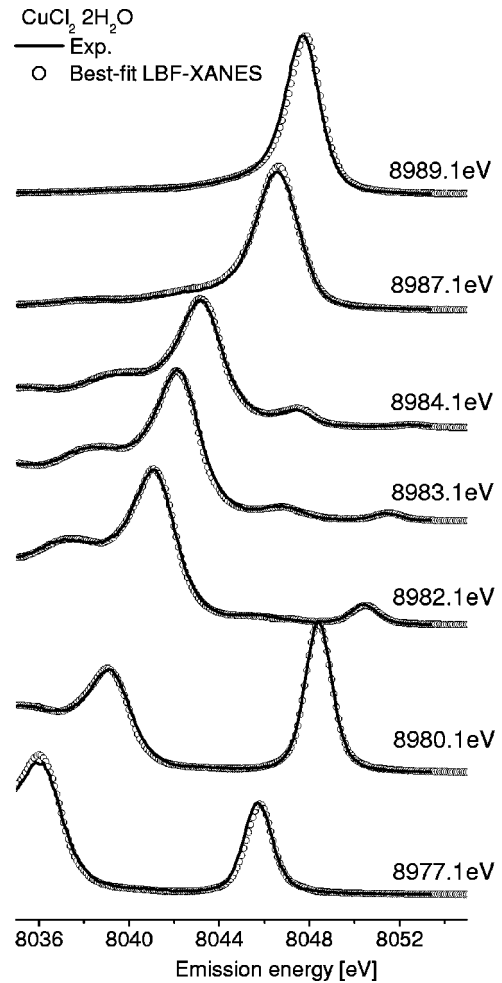
weak scattering intensity at off-resonant conditions requires a long data accumulation period, which imposes some restrictions for a wide application of the technique. Now it has been proved that LBS/LBF-XANES can be deduced from a RIXS spectrum obtained under close-to-resonant conditions (a few eV below the edge). The advantage of employing close-to-resonant conditions is obvious: a 2–3 orders of magnitude intensity gain is achieved. An apparent disadvantage is that some calculations are required to deduce the LBS/LBF-XANES spectrum from RIXS. Since the calculation is straightforward and can be carried out almost without resorting to any unambiguous or uncertain parameters, the advantage far exceeds the disadvantage and warrants a wide application of this method.

Compared with the HRFE spectroscopy, the present method has several advantages also, in addition to the fact that the resolution is limited only by $\Delta E_{\text{expt}}$ and $\Gamma_{2p}$ (analytical method: LBS) or by $\Delta E_{\text{expt}}$ (simulation method: LBF), as has already been discussed. The first is that not only focusing-type spectrometers but also dispersive-type spectrometers can be used, which makes it possible to extend the number of atomic species that can be studied, the reason being discussed in some detail in the previous publication.[12]

Second, since both the incident energy and scattering energy are below the absorption edge, absorption is relatively weak and changes only slightly with excitation energy, while during a scan in the HRFE spectroscopy absorbance varies drastically. This makes the difference of LBS/LBF-XANES spectra of the two at higher energies as shown in Figs. 9(a) and 9(b).

Finally, the excitation energy is fixed in the LBS/LBF-XANES by RIXS. Hence, if a dispersive-type spectrometer equipped with position-sensitive detector is employed, the accumulated data are free from any temporal fluctuations. More importantly, it makes it much easier to incorporate this method with other techniques—for example, x-ray diffraction.

Since the closer to resonance, the more intense the scattering is, a use of higher excitation energy is preferable. From the simplified model shown in Fig. 1, LBS/LBF-XANES can be derived from RIXS obtained by exciting with $\omega_1 < \Omega_{1s} - \Gamma_{1s}/2\hbar$. In practice, however, the absorption edge is not a step function, and hence lower excitation energy must be employed, making the scattering intensity somewhat weak. This slight disadvantage will, however, fully be compensated for by the use of a dispersive-type spectrometer combined with plural analyzer crystals and a position-sensitive detector. A new spectrometer based on this idea is now under construction.

---

*Corresponding author. FAX: +81-22-217-5405. Electronic address: hayashi@tagen.tohoku.ac.jp

†Present address: JASRI, Mikazuki, Hyogo 679-5198, Japan.

‡Present address: Semiconductor Energy Laboratory Co., Ltd., Hase 398, Atsugi, Kanagawa, 243-0036, Japan.

[1] M.O. Krause and J.H. Oliver, J. Phys. Chem. Ref. Data **8**, 329 (1979).

[2] K. Hämäläinen, D.P. Siddons, J.B. Hastings, and L.E. Berman, Phys. Rev. Lett. **67**, 2850 (1991).

[3] P. Carra, M. Fabrizio, and B.T. Thole, Phys. Rev. Lett. **74**, 3700 (1995).

[4] P.W. Loeffen, R.F. Pettifer, S. Müllender, M.A. van Veenendaal, J. Röhler, and D.S. Sivia, Phys. Rev. B **54**, 14 877 (1996).

[5] A. Kotani and S. Shin, Rev. Mod. Phys. **73**, 203 (2001).

[6] J. Tulkki and T. Åberg, J. Phys. B **15**, L435 (1982).

[7] P. Suortti, V. Eteläniemi, K. Hämäläinen, and S. Manninen, J. Phys. (Paris), Colloq. **48**, C9-831 (1987).

[8] V. Eteläniemi, K. Hämäläinen, S. Manninen, and P. Suortti, J. Phys.: Condens. Matter **4**, 879 (1992).

[9] Y. Udagawa and K. Tohji, Chem. Phys. Lett. **148**, 101 (1988).

[10] Y. Udagawa, H. Hayashi, K. Tohji, and T. Mizushima, J. Phys. Soc. Jpn. **63**, 1713 (1994).

[11] H. Hayashi, Y. Udagawa, W.A. Caliebe, and C.-C. Kao, Phys. Rev. B **66**, 33 105 (2002).

[12] H. Hayashi, Y. Udagawa, W.A. Caliebe, and C.-C. Kao, Chem. Phys. Lett. **371**, 125 (2003).

[13] N. Kosugi, H. Kondoh, H. Tajima, and H. Kuroda, Chem. Phys. **135**, 149 (1989).

[14] N. Kosugi, T. Yokoyama, K. Asakura, and H. Kuroda, Chem. Phys. **91**, 249 (1984).

[15] H.J. Milledge, *International Tables for X-ray Crystallography* (The International Union of Crystallography, Tokyo, 1985).